

## Energy distribution measurements in radio frequency plasma discharges using a cubical analyzer

Phi Long Nguyen, R. B. Turkot, and D. N. Ruzic

Citation: *J. Vac. Sci. Technol. A* **9**, 682 (1991); doi: 10.1116/1.577343

View online: <http://dx.doi.org/10.1116/1.577343>

View Table of Contents: <http://avspublications.org/resource/1/JVTAD6/v9/i3>

Published by the AVS: Science & Technology of Materials, Interfaces, and Processing

### Related Articles

Can surface cracks and unipolar arcs explain breakdown and gradient limits?

*J. Vac. Sci. Technol. A* **31**, 011302 (2013)

Mechanically robust silica-like coatings deposited by microwave plasmas for barrier applications

*J. Vac. Sci. Technol. A* **30**, 061502 (2012)

Spatially resolved measurements of ion density and electron temperature in a dual-frequency capacitively coupled plasma by complete floating double probe technique

*J. Vac. Sci. Technol. A* **29**, 011006 (2011)

High etching rates of bulk Nb in Ar/Cl<sub>2</sub> microwave discharge

*J. Vac. Sci. Technol. A* **27**, 301 (2009)

Study of fluorocarbon plasma in 60 and 100MHz capacitively coupled discharges using mass spectrometry

*J. Vac. Sci. Technol. A* **26**, 1198 (2008)

### Additional information on *J. Vac. Sci. Technol. A*

Journal Homepage: <http://avspublications.org/jvsta>

Journal Information: [http://avspublications.org/jvsta/about/about\\_the\\_journal](http://avspublications.org/jvsta/about/about_the_journal)


Top downloads: [http://avspublications.org/jvsta/top\\_20\\_most\\_downloaded](http://avspublications.org/jvsta/top_20_most_downloaded)

Information for Authors: [http://avspublications.org/jvsta/authors/information\\_for\\_contributors](http://avspublications.org/jvsta/authors/information_for_contributors)

## ADVERTISEMENT


# Instruments for advanced science

**Gas Analysis**




- dynamic measurement of reaction gas streams
- catalysis and thermal analysis
- molecular beam studies
- dissolved species probes
- fermentation, environmental and ecological studies

**Surface Science**




- UHV TPD
- SIMS
- end point detection in ion beam etch
- elemental imaging - surface mapping

**Plasma Diagnostics**



- plasma source characterization
- etch and deposition process reaction kinetic studies
- analysis of neutral and radical species

**Vacuum Analysis**




- partial pressure measurement and control of process gases
- reactive sputter process control
- vacuum diagnostics
- vacuum coating process monitoring

contact Hiden Analytical for further details

**HIDEN ANALYTICAL**

[info@hideninc.com](mailto:info@hideninc.com)  
[www.HidenAnalytical.com](http://www.HidenAnalytical.com)

CLICK to view our product catalogue 

# Energy distribution measurements in radio frequency plasma discharges using a cubical analyzer

Phi Long Nguyen,<sup>a)</sup> R. B. Turkot, Jr., and D. N. Ruzic

Department of Nuclear Engineering, University of Illinois, Urbana, Illinois 61801

(Received 8 October 1990; accepted 3 December 1990)

A compact and inexpensive cubical energy analyzer has been developed to measure ion and electron energy distributions at the boundaries of a rf plasma. It consists of two grids parallel to the plasma boundary behind which lies a  $1\text{ cm} \times 1\text{ cm} \times 1\text{ cm}$  cube. The absorbed current and voltage on the grids and on each face of the cube can be monitored and biased independently. A Helmholtz coil on the outside of the cube allows a 0–15 G field to be produced perpendicular to the path through the gridded apertures. The advantages over standard gridded energy analyzers include direct measurements of ion-induced secondary electrons and separation of electrons, negative ions, and heavy and light mass positive ions to different collection surfaces. Measurements of the ion and electron energy distributions at the grounded electrode of a parallel plate 13.56 MHz plasma discharges clearly show a time-varying rf sheath and a non-Maxwellian electron energy distribution. Data is presented for Ar, CH<sub>4</sub>, and H<sub>2</sub> plasmas.

## I. INTRODUCTION

Weakly ionized plasmas are used extensively in processing of semiconductor integrated circuits.<sup>1</sup> One of the obstacles to understanding weakly ionized plasma processes is the determination of the energy distributions of electrons and ions that exist in the bulk plasma and near the plasma–surface interface. Maxwell–Boltzman electron energy distributions only arise in electric-field-free plasmas dominated by elastic collisions and where the collision frequency is not a strong function of energy. In weakly ionized plasmas inelastic collisions, especially excitation, dominate and deplete the tails of the bulk energy distributions. Strong electric fields also exist in the sheaths at each electrode, which accelerate ions to the surfaces. As a consequence secondary electrons are ejected, which are accelerated into the plasma. These sheath regions can extend over a few centimeters<sup>2</sup> and often comprise half or more of the discharge volume.

Direct measurement of the electron energy distribution would allow determination of plasma parameters such as process rate constants, transport coefficients, and electron densities. Knowledge of the ion energy distribution at the plasma–surface interface would allow better characterization of etching, sputtering, and dangling bond formation. Electron energy distributions can be determined in principle from the second derivative of a Langmuir probe  $I-V$  characteristic.<sup>3</sup> However, this technique is complicated by intrusion of the probe into the plasma, secondary electron emission from the probe, time-varying effects, and negative ions. Mass spectroscopic techniques<sup>4</sup> are well suited for study of ions at the surface, but typically require differential pumping, considerable space, and high cost.

To overcome the limitations of Langmuir probes and mass spectrometers, a type of gridded energy analyzer was constructed to fit within the grounded electrode of a commercial parallel-plate 13.56 MHz plasma processing device. The analyzer consists of two stainless steel plates with 1 mm diam apertures parallel to the plasma boundary, behind

which lies a  $1\text{ cm} \times 1\text{ cm} \times 1\text{ cm}$  cube. The aperture closest to the plasma is covered with a fine mesh grid. The absorbed current and voltage on the plates and on each face of the cube can be monitored and biased independently. A Helmholtz coil on the outside of the cube allows a 0–15 G field to be produced perpendicular to the path through the apertures. The electrical separation of each cube face allows electric fields to be created in the  $x$ ,  $y$ , and  $z$  planes. Correct combinations of  $E_x$ ,  $E_y$ ,  $E_z$ , and  $B_x$  separate heavy positive ions, light positive ions, negative ions, plasma electrons, and secondary electrons generated within the cube to differing collection surfaces. The first two plates allow energy distributions to be discriminated.

This paper shows mostly “conventional” ion and electron energy distributions obtained by varying the grid potentials and monitoring the currents to all interior faces of the cube. Ion energy results are similar to those from other retarding field energy analyzers in rf plasmas.<sup>5–7</sup> Electron energy distributions show a strong time-varying beam component in agreement with previous rf probe work.<sup>8–10</sup>

## II. APPARATUS

This research was performed on a Davis & Wilder model 425 parallel plate plasma etcher powered by a Plasma-Therm HFS 2000E, 2 kW 13.56 MHz generator. The parallel plates are 70.1 cm in diameter and are 3.7 cm apart. Quartz plates lie above the top (powered) electrode and around the circumference of the plasma. This leads to roughly equal electrode areas and virtually no dc offset between the electrodes. Gas was flowed through the system at approximately 4 SCCM. More details of the plasma device, matching network, power diagnostics, and grounding system can be found in earlier papers.<sup>9,10</sup>

The cubical energy analyzer was placed just below the grounded (bottom) electrode at a radial location 25 cm from the center. It is actually embedded in the electrode between

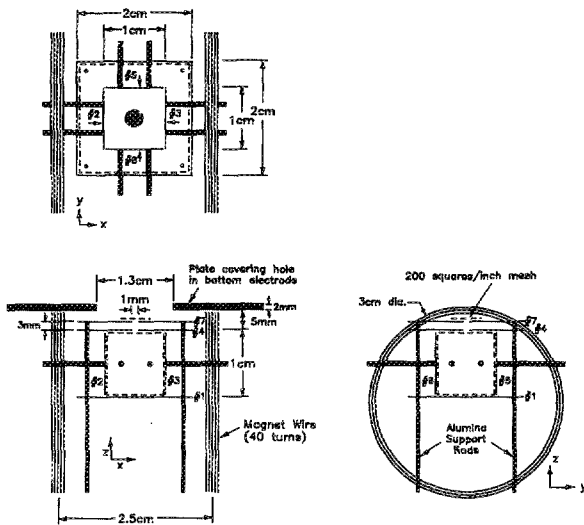


FIG. 1. Top and side views of the cubical analyzer. The support rods were attached to the cube faces with a vacuum epoxy. The probe head is shielded from the plasma by a thin copper cover. The entire support structure is not shown.

the water cooling coils in order to minimize the distance between the probe's first aperture and the plasma. Figure 1 shows the top and both side views of the cubical probe. It was designed such that each face is electrically isolated from all others. There is a 200 mesh screen over the 1 mm aperture in the uppermost plate (grid #7). The next 1 mm aperture is in the top of the cube (plate #4) and does not have a screen. The base of the cube (plate #1) and its four sides (plates #2, #3, #5, and #6) form a 1 cm  $\times$  1 cm  $\times$  1 cm cavity. The analyzer is built from high precision machined stainless steel Electron Volts Parts™. The cubical cavity was formed around four alumina rods, 1.5 mm in diameter. Stainless steel structures were then erected around the alumina support structure and held together by alumina washers, stainless steel compression springs, and Torr Seal™, a vacuum-compatible epoxy. Two short stainless steel rods were cemented to each side plate and held in place by the insulated support structure. Twenty-two gauge Ni wires were spot welded onto the collection plates and connected to the center conductor of individually shielded cables.

The cables pass through the bottom of the chamber and to the collection circuitry located in a shielded room. Each of the seven plates can be biased positively or negatively. A Fluke model 75 multimeter measures the voltage drop across its 10 M  $\Omega$  input resistance to determine the current drawn by each plate. Identical current readings were obtained using a floating Keithly model 415 A picoammeter.

A pair of 3-cm-diam magnetic coils were placed at the side of the analyzer's cavity. The coils each have 40 turns of 28-gauge Belden copper magnet wire and are separated by 2.5 cm. The magnetic field was calibrated and its uniformity measured with a Walker Scientific MG-5D gauss meter prior to installation. Over the width of the cube the field varies 20%. The absence of active cooling on the coils limits the fields to 15 G in the steady state.

The entire analyzer is shielded from the plasma by wrapping it in 1 ml Mylar™ and Scotch™ copper tape. Soft solder was used to ensure dc continuity between the copper tape strips. The probe is pumped through its aperture and through a gap near the bottom of the chamber where the signal and magnet wires emerge from the shielding. More details of the probe construction and measurement circuitry are given in Ref. 11.

### III. MODELING

Particle motion in crossed electric and magnetic fields was modeled for the probe's interior. Though the magnetic field varies by less than 20% across the cube in a simple manner, an application of a voltage to one of the faces does not provide a uniform electric field in the probe's interior. Since each face of the cube can be at a different potential, Poisson's equation is solved for a cube with one corner at the origin and sides of length  $a$ , which has the  $z = a$  face at potential  $V$  and all other faces at potential 0. The solution is

$$\Phi(x,y,z) = \sum_{n=1,3,\dots}^{\infty} \sum_{m=1,3,\dots}^{\infty} \frac{16V \sinh(\gamma_{nm}z)}{m\pi a \sinh(\gamma_{nm}a)} \times \sin\left(\frac{n\pi x}{a}\right) \sin\left(\frac{m\pi y}{a}\right),$$

where

$$\gamma_{nm} = \pi[(n^2 + m^2)/a^2]^{1/2}.$$

The solutions are superimposed to find the true potential distribution within the cube for a given setting of  $V_1$  through  $V_6$ . Once the potential is determined the electric field components are found from the partial derivatives of the potential. Knowledge of the exact  $E(x,y,z)$  and  $B(x,y,z)$  allows the trajectories of any charged particle to be calculated. However, for most situations the assumption of uniform electric fields gives the same results as the exact fields.

As an example of particle separation consider the case of  $V_1 = +65$ ,  $V_2 = +120$  and  $V_3$  through  $V_7$  at 0. Energetic electrons that enter the cube will curve only slightly toward plate #2 on their way to being collected on plate #1 while negative ions will be attracted to plate #2. Positive ions will be collected on plate #3. The addition of a magnetic field will deflect very low energy electrons to plate #5, especially if the potentials on plates #1 and #2 are lowered.

Since the probe is not differentially pumped, collisions and even ionizations within the cube must be considered. Assuming a scattering cross section<sup>12</sup> of  $1 \times 10^{-15}$  cm<sup>2</sup> a pressure of 6 mTorr has a mean-free path of 6.9 cm. At 100 mTorr, used for the bulk of the experiments presented here, the collision mean-free path drops to 0.4 cm. Most ion-neutral scattering collisions, however, are very forward peaked so deflections by neutral atoms inside the probe are not expected to have a major influence. Charge exchange reactions in the cube are also likely to occur at 100 mTorr. Any ions that charge exchange will still be drawn to one of the interior plates because the potential of plate #4 is higher than than the other portions of the cube during the ion collection experiments. Due to these two scattering effects, the currents

to the interior of the cube (plates #1–6) were summed for the 100 mTorr data.

Electron ionization cross sections are better known, but quite sensitive to energy. Given a cross section<sup>13</sup> of  $1.8 \times 10^{-16} \text{ cm}^2$  at 30 eV, the mean-free path for electrons in Ar is 38 cm at 6 mTorr and 2.3 cm at 100 mTorr. To account for the small number of ionizations that still may occur inside the probe the interior currents were summed when determining the electron energy distributions as well.

#### IV. RESULTS

The first experiments were conducted at  $100 \pm 5 \text{ W}$  forward power and  $20 \pm 5 \text{ W}$  reflected in  $6 \pm 1 \text{ mTorr}$  Ar. The bias on plate #5 was varied from 0 to +365 while the current on all other faces was monitored. The initial positive signal on plate #1 increased slightly (about 8%) as ion-induced secondary electrons were pulled to plate #5. The signal on plate #1 then dropped, the ion signal on plate #6 rose and the electron signal on plate #5 rose as the electric field increased.

With the ions going to plate #6 and the electrons going to plate #5, plate #4 could now be used as an energy discriminator by raising its potential from 0–105 V. Figure 2 shows the raw unsmoothed data and the ion energy distribution found from differentiating the collected current and performing one three-point smoothing on the resulting derivative curve.

A combination of rf Langmuir probes and capacitive probes were also used in the same discharge following Ref. 9. The electron density was  $4.1 \pm 1.1 \times 10^9 \text{ cm}^{-3}$ . Even though the electron energy distribution was not Maxwellian, standard analysis of the exponential portion of the probe characteristic yielded an electron "temperature" of  $8.8 \pm 0.4 \text{ eV}$ .

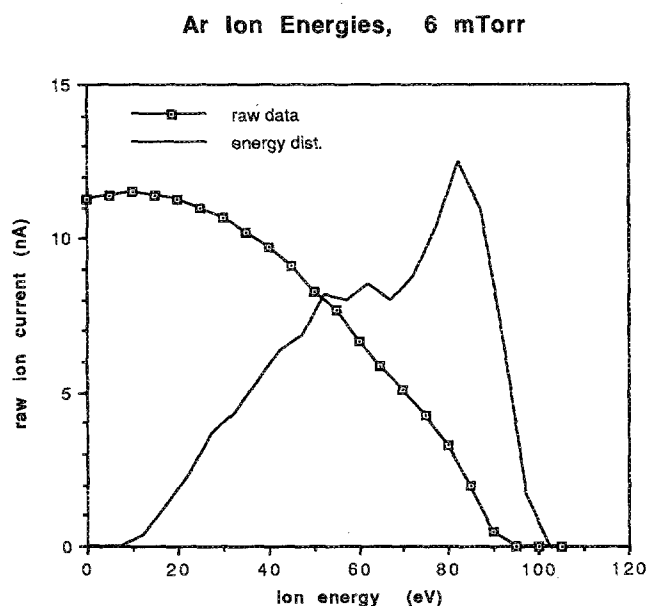


FIG. 2. Current on plate #6 as a function of voltage on plate #4, and the ion energy distribution on the grounded electrode for a  $6 \pm 1 \text{ mTorr}$ ,  $80 \pm 7 \text{ W}$  Ar plasma.

The dc average of the time varying plasma potential was found to be  $96 \pm 3 \text{ V}$ . This compares favorably with the cut-off of the ion energy distribution obtained with the cubical probe (see Fig. 2.)

At higher pressures the physical width of the sheath drops considerably<sup>2</sup> and the transit time of an Ar ion through the sheath decreases, even though its energy is less. At 6 mTorr the argon ion experiences approximately 25 rf periods<sup>14</sup> as it transverses the sheath. At 100 mTorr this drops to approximately 15 periods and the response due to instantaneous plasma potentials may begin to be seen. Lighter ions such as  $\text{CH}_x^+$  and  $\text{H}^+$  spend even less time in the sheath: approximately 10 and 2.5 periods, respectively, and should show the instantaneous minimum and maximum plasma potentials more clearly.<sup>15</sup>

Figure 3 shows raw ion currents and differentiated and smoothed ion energy distributions for Ar,  $\text{CH}_4$ , and  $\text{H}_2$  plasmas all taken at  $100 \pm 5 \text{ mTorr}$ ,  $100 \pm 5 \text{ W}$  forward power, and less than 5 W reflected power. Due to the increased ion scattering at the higher pressure the data was taken using the interior of the cube as a Faraday cup: the currents on the interior plates were summed. Grid #7 was biased 70 V negative to repel the electrons and plate #4 was used as a discriminator in the 0 + 60 V range. The emergence of the ion energy peak due to the plasma potential minimum is clearly seen. The degradation of the higher energy peak in the  $\text{H}_2$  plasma spectrum may be due to  $\text{H}^+$  and  $\text{H}_2^+$  reaction cross sections, which increase with increasing ion energy.

Based on the plasma potential values discernible from Fig. 3, electron energy distribution measurements were attempted. Figure 4 shows the analyzer voltage settings used to collect electron data from the 100 mTorr Ar plasma. Grid #7 was biased to the plasma potential maximum of 35 V, the maximum ion energy seen in Fig. 3(a). Setting grid #7 to 35 V also maximized the electron current obtained on plate #4 ( $V_4 = 0$ ). To reject ions and to accelerate electrons into the cube, plate #4 was raised to +70 V. The energy distribution was obtained by monitoring the current to all inside surfaces and biasing plate #1 between 40 and -25 V. When plate #1 was biased negative, plates #2, #3, #5, and #6 were also brought negative to minimize the deflection of any remaining electrons. The raw data and once smoothed differentiated distributions are shown in Fig. 5. A host of electron energy peaks are seen. A possible explanation is given in the next section.

#### V. DISCUSSION

There are two components of the electron energy distribution in a low-pressure parallel-plate rf discharge: (1) a bulk electron population that is often represented by a Maxwellian distribution, and (2) a beam electron population created by ion-induced secondary emission from the electrodes and subsequent acceleration in the instantaneous plasma sheath. This energetic constituent is termed a beam because the electrons are all initially directed away from the ion-bombarded surface.

The instantaneous minimum and maximum plasma potentials in an Ar rf plasma<sup>9</sup> for this device are schematically represented in Fig. 4. The flat portions of the potentials at 10

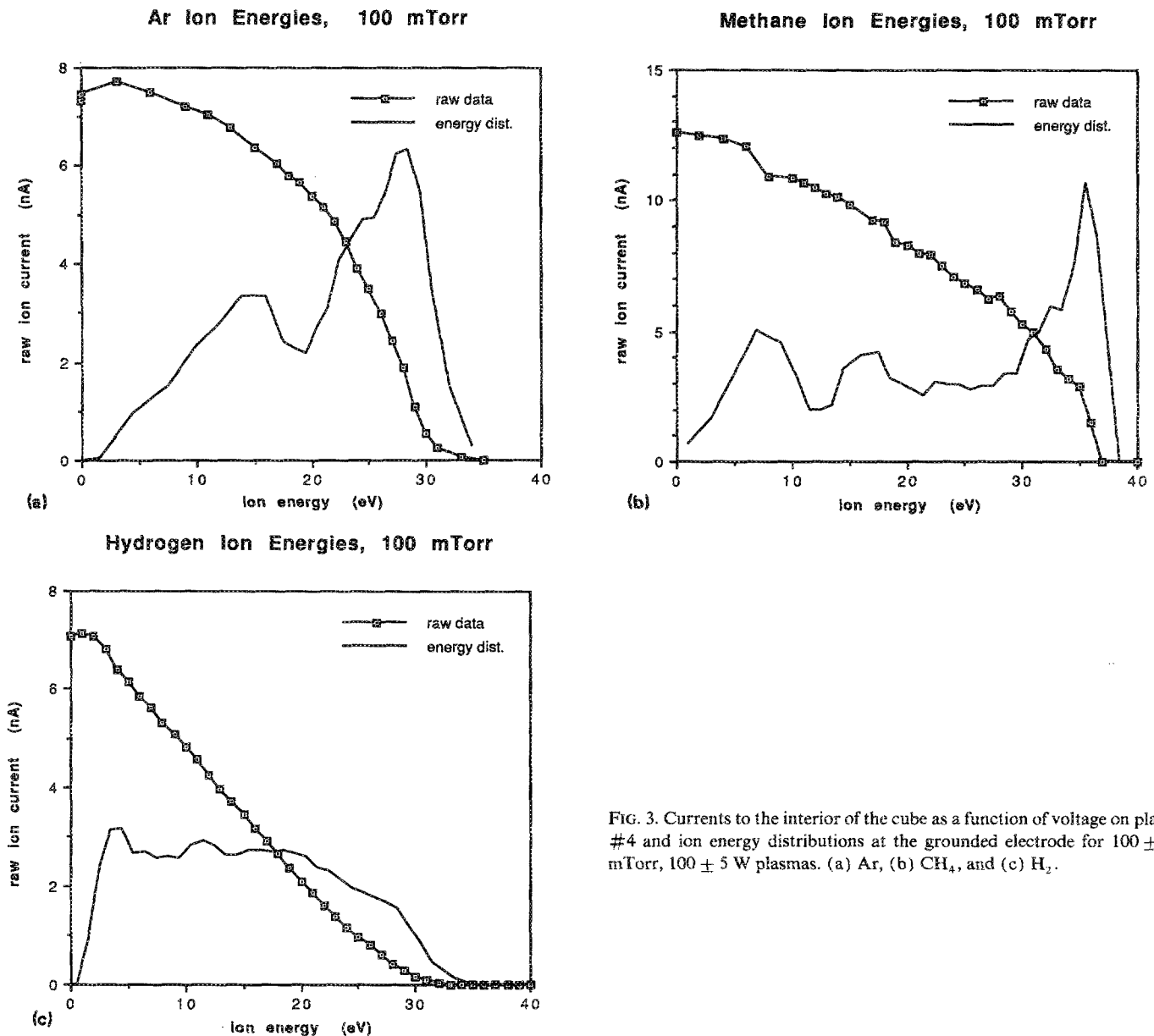


FIG. 3. Currents to the interior of the cube as a function of voltage on plate #4 and ion energy distributions at the grounded electrode for  $100 \pm 5$  mTorr,  $100 \pm 5$  W plasmas. (a) Ar, (b)  $\text{CH}_4$ , and (c)  $\text{H}_2$ .

and 35 eV were approximated by the peaks of the ion energy distribution. The potentials at the powered electrodes are somewhere in the range of  $\pm 30$  to  $\pm 10$  V. The value of  $\pm 20$  is depicted. During the minimum of the plasma potential a strong beam component will be created at the powered electrode. Referring to Fig. 4, those beam electrons that cross the plasma and reach grid #7 will have a maximum of 55 eV [ $55 = 35 - (-20)$  V]. During the maximum of the plasma potential a smaller beam component will be launched from the powered electrode due to the lower ion energy. Those beam electrons that reach grid #7 will have 15 eV [ $15 = 35 - (+20)$  V]. Therefore the beam electron distribution measured in this experiment should have a larger peak near 55 eV and a smaller peak at 15 eV with some electrons with energies in between.

The bulk electron energy distribution will also be seen. Measurements show an electron "temperature" of around  $3 \text{ eV}^{10}$  for these conditions. At the time of maximum plasma potential, this distribution would be seen directly at grid #7

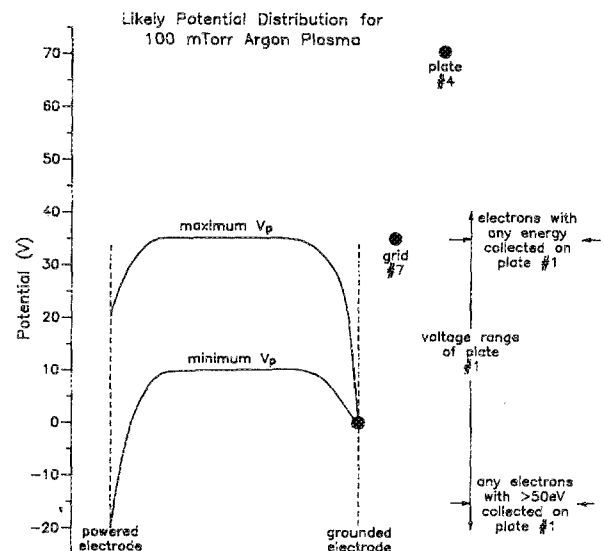


FIG. 4. Potential distribution across the Ar plasma that could result in the electron energy distribution collected with grid #7 biased to 35 V and plate #4 biased to 70 V.

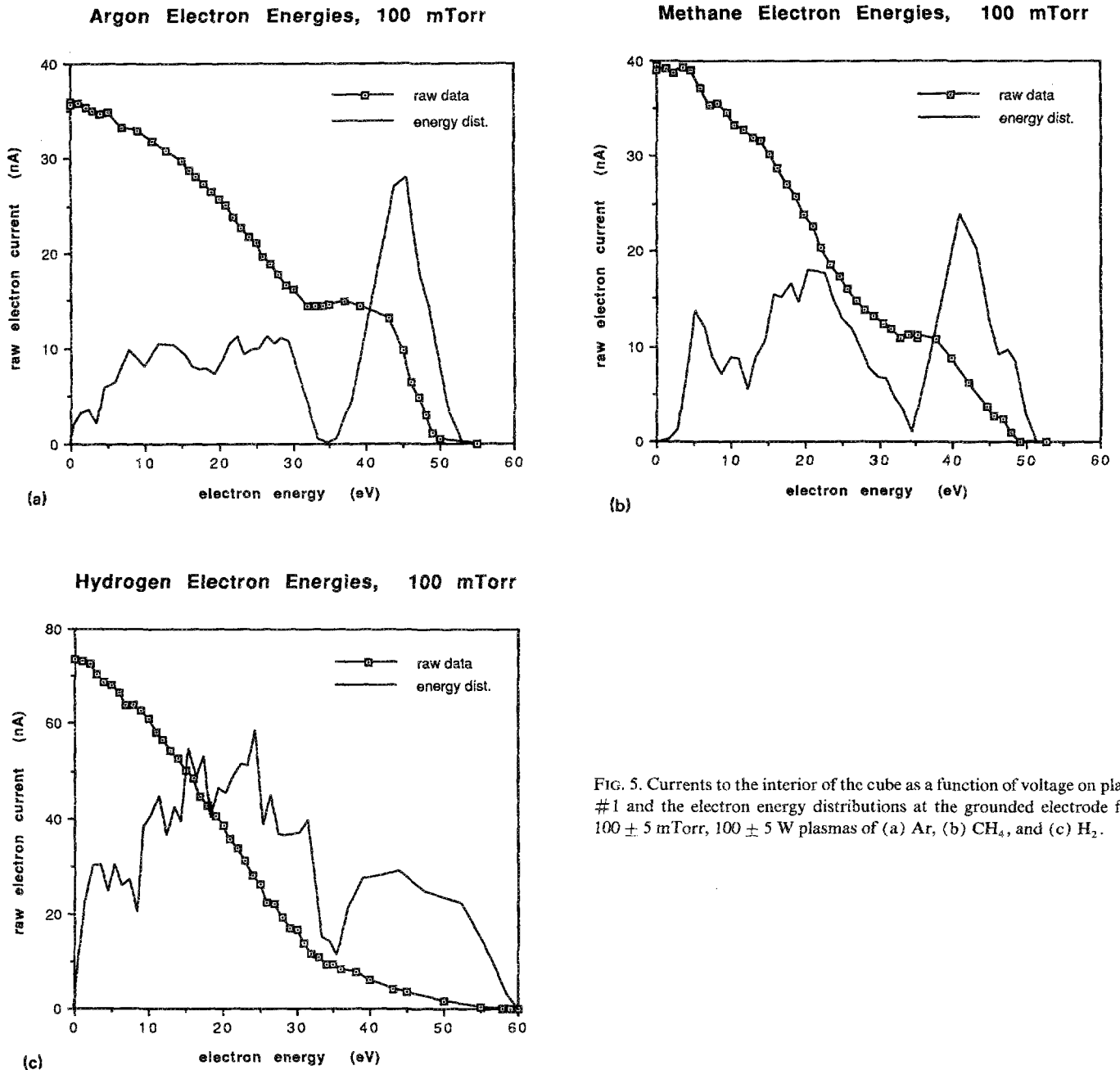


FIG. 5. Currents to the interior of the cube as a function of voltage on plate #1 and the electron energy distributions at the grounded electrode for  $100 \pm 5$  mTorr,  $100 \pm 5$  W plasmas of (a) Ar, (b)  $\text{CH}_4$ , and (c)  $\text{H}_2$ .

giving a rounded peak mainly between 0 and 7 eV. At the time of minimum plasma potential, the bulk distribution would be accelerated by an additional 25 eV [ $25 = 35 - (+10)$  V], giving a broad peak in the 25–32 eV range. This distribution due to the bulk electrons will also have some energies between the two broad peaks. Superimposing the bulk and beam time-varying distributions gives a shape similar to that seen in Fig. 5. When the experiment was repeated for  $\text{CH}_4$  and  $\text{H}_2$  similar electron energy distribution features resulted. The  $\text{H}_2$  results showed a smaller signal at the maximum energies just as the  $\text{H}_2$  ion energy distribution showed.

This work introduces a novel and compact energy analyzer potentially useful for plasma processing applications. Using the analyzer confirms the existence of time-varying potentials in a rf discharge and the existence of electron beams.

Future work will include the installation of a mu-metal shield between the coils and the plasma so application of a  $B$  within the cube does not alter the sheath dynamics. Negative ions will also be addressed with the use of an electronegative gas such as  $\text{CF}_4$  or  $\text{SF}_6$ .

#### ACKNOWLEDGMENTS

This work was supported by Intel corporation through the donation of the plasma etcher, IBM corporation through the donation of the rf power supply, DOE Subcontract No. 19XSF633V with ORNL, and NSF Grant No. CBT-84-51599.

<sup>a)</sup> Present address: Intel Corporation, Hillsboro, Oregon 97123.

<sup>1</sup> *Handbook of Plasma Processing*, edited by S. M. Rosnagel, J. J. Cuomo, and W. D. Westwood (Noyes, Park Ridge, NJ, 1990).

- <sup>2</sup>N. Mutsukura, K. Kobayashi, and Y. Machi, *J. Appl. Phys.* **68**, 2657 (1990).
- <sup>3</sup>J. W. Swift and M. J. R. Schwar, *Electrical Probes for Plasma Diagnostics* (Hilffe Books, London, 1970).
- <sup>4</sup>W. D. Davis and T. A. Vanderslice, *Phys. Rev.* **131**, 219 (1963).
- <sup>5</sup>W. M. Greene, M. A. Hartney, W. G. Oldham, and D. W. Hess, *J. Appl. Phys.* **63**, 1367 (1988).
- <sup>6</sup>A. D. Kuypers and H. J. Hopman, *J. Appl. Phys.* **63**, 1894 (1988).
- <sup>7</sup>A. M. Smith, B. N. Beilby, and C. M. Horwitz, *J. Vac. Sci. Technol. A* **7**, 3332 (1989).
- <sup>8</sup>J. L. Wilson, J. B. O. Caughman II, P. L. Nguyen, and D. N. Ruzic, *J. Vac. Sci. Technol. A* **7**, 972 (1989).
- <sup>9</sup>D. N. Ruzic and J. L. Wilson, *J. Vac. Sci. Technol. A* **8**, 3746 (1990).
- <sup>10</sup>D. N. Ruzic, S. L. Balog, and R. B. Turkot, Jr., in *Proceedings of the 12th Dry Processing Symposium* (Tokyo, Japan, 1990).
- <sup>11</sup>P. L. Nguyen, Master's thesis, University of Illinois, Department of Nuclear Engineering, 1990.
- <sup>12</sup>D. N. Ruzic and S. A. Cohen, *J. Chem. Phys.* **83**, 5527 (1985).
- <sup>13</sup>B. Chapman, *Glow Discharge Processes* (Wiley, New York, 1980).
- <sup>14</sup>Y. Okamoto and H. Tamagawa, *J. Phys. Soc. Jpn.* **27**, 270 (1969).
- <sup>15</sup>M. J. Kushner, *J. Appl. Phys.* **58**, 4024 (1985).